Bioprinting 13 (2019) e00041

Contents lists available at ScienceDirect

Bioprinting

journal homepage: www.elsevier.com/locate/bprint

Bioprinting exosome-like extracellular vesicle microenvironments

Saigopalakrishna S. Yerneni[a], Theresa L. Whiteside[b], Lee E. Weiss[c], Phil G. Campbell[d,*]

[a] Department of Biomedical Engineering, Carnegie Mellon University, Pittsburgh, PA, USA
[b] Departments of Pathology, Immunology and Otolaryngology, University of Pittsburgh School of Medicine and UPMC Hillman Cancer Center, Pittsburgh, PA, USA
[c] The Robotics Institute and Department of Biomedical Engineering, Carnegie Mellon University, Pittsburgh, PA, USA
[d] Department of Biomedical Engineering and Engineering Research Accelerator, Carnegie Mellon University, Pittsburgh, PA, USA

ARTICLE INFO

Keywords:
Extracellular vesicle
Exosome
Extracellular matrix
Bioprinting
Macrophage
Myogenesis

ABSTRACT

Exosomes are a subset of extracellular vesicles that transport a wide variety of cell signaling molecules. Similar to growth factors, exosomes occur both in a 'liquid-phase' suspension in body fluids and in a 'solid-phase' immobilized *via* native binding affinities to the extracellular matrix (ECM). To date, most investigations have been focused on liquid-phase exosomes, and only limited information is available regarding the interaction between exosomes and the ECM components during intercellular communication. This gap in knowledge is partly due to the lack of well-defined *in vitro* models of solid-phase exosome/ECM microenvironments. To study these interactions, we adapted our inkjet-based bioprinting technology to fabricate spatially defined patterns of solid-phase exosome microenvironments. As a paradigm application, microenvironments consisting of exosomes derived from different macrophage subsets, M0 (non-activated), M1 (pro-inflammatory) and M2 (pro-regenerative), were bioprinted on collagen type-I coated substrates and their effects on myogenesis of C2C12 cells were investigated in registration to the printed patterns. M1 exosome microenvironments spatially inhibited myogenesis while promoting proliferation, whereas M2 exosome microenvironments spatially promoted myogenesis in a dose-dependent manner. This work provides the proof-of-concept for bioprinting highly controlled and well-defined exosome-based microenvironments that can be used to investigate mechanisms underpinning exosome-mediated effects on the ECM. Furthermore, this bioprinting technology can be directly translated to *in vivo* applications for localized exosome delivery to tissues.

1. Introduction

Extracellular vesicles (EVs) are a heterogeneous population of vesicles encapsulated by a protein-phospholipid membrane. EVs range in size from nanometers to microns and are produced by all nucleated cells as well as erythrocytes and platelets. Consequently, EVs are present in all body fluids and mediate local and systemic intercellular communication in health and disease [1–3]. EVs carry and deliver to recipient cells rich molecular signaling cargos, including membrane-associated signaling molecules as well as nucleic acids, enzymes and growth factors within the vesicle lumen. Upon delivery of the cargo, EVs re-program recipient cells, altering their functions through extracellular cell surface receptor ligand-like interactions and/or by intracellular uptake of nucleic acids and other biologically-active molecules/factors [1–4]. The cargo of EVs and their ability to re-program recipient cells varies depending on the parent cell type, ability of the recipient cells to take up EVs and the cellular microenvironment. EV-mediated cell-to-cell communication plays a critical role in both normal and pathophysiological conditions.

Exosomes, which are a subset of EVs [4], are 30–150 nm in diameter and originate from the endocytic compartment (*i.e.* multivesicular bodies) of the parent cell. Exosomes are receiving ever-increasing interest because of their potential to serve as disease biomarkers and as therapeutic targets. Thus, exosomes could be used for delivery of their inherent cargo as well as exogenously-loaded cargo to diseased cells or tissues [1,5–7]. Compared to the polymeric and liposomal-based nanoparticle delivery approaches that have been used for the last 40 years to treat a broad range of pathologies [8–10], exosomes hold promise as ideal delivery vehicles because they are naturally occurring nanovesicles evolved explicitly for intercellular communication. Furthermore, protection of the exosome cargo constituents from extracellular antagonists and synergistic interactions between a loaded 'drug' cargo and endogenous co-cargo constituents may represent advantages over traditional single-drug delivery strategies.

Similar to growth factors, exosomes exist both in soluble liquid-phase form and in immobilized solid-phase form bound within the extracellular matrix (ECM). However, essentially all research to date

* Correspondence to: Carnegie Mellon University, Scott Hall 6115, 5000 Forbes Avenue, Pittsburgh, PA 15213, USA.
E-mail address: pcampbel@cs.cmu.edu (P.G. Campbell).

https://doi.org/10.1016/j.bprint.2019.e00041
Received 15 October 2018; Received in revised form 10 January 2019; Accepted 11 January 2019

regarding exosomes has focused on exosomes present in body fluids. The association of exosomes within the ECM is less understood, and, overall, little is known about interactions between exosomes and the ECM components during intercellular communication [11]. Exosomes readily bind to ECM molecules such as fibronectin [12–14] and collagen [13]. In cancer, exosomes bind and modulate the ECM [15] and have been identified in association with collagen fibrils within tumor tissues [16]. The role of tumor-derived exosomes in immune suppression and cancer progression has been intensively investigated [17,18].

Solid-phase exosomes form localized exosome-based microenvironments. Within these microenvironments, the sequestered exosomes direct cell signaling *via* their signaling cargo, similar to solid-phase growth factors, as previously described [19]. The mechanisms of these interactions between exosomes and the ECM components that presumably determine the extent of exosome-driven reprogramming in tissues are not understood. Therefore, gaining a better understanding of solid-phase exosome biology has implications for the future development of exosome-based therapeutics. *In vitro* models that recapitulate immobilized exosome/ECM microenvironments are needed for these investigations. Such microenvironments could also serve as screening tools to evaluate candidate exosome-based therapeutics prior to *in vivo* studies. Moreover, engineering solid-phase exosome microenvironments using a technology that can be directly translated to fabricating implantable constructs has implications toward localized delivery of exosome-based therapeutics. Here, we report the adaptation of our established inkjet-based biopatterning technology [20–24] to create exosome/ECM microenvironments.

We originally pioneered biopatterning technology based on biomimicry to engineer microenvironments with protein and peptide-based signaling molecules, and their response modifiers, to recapitulate aspects of biological spatial patterning of cell functions. Such patterning occurs during embryogenesis and throughout development [25,26], as well as during normal tissue maintenance and wound healing [27,28]. We have previously demonstrated controlled deposition of defined patterns of growth factor bioinks on and in native ECM-based substrates. Native binding of the growth factors to the ECM components results in the formation of defined solid-phase growth factor patterns that are retained for sufficient periods of time to signal cells, both *in vitro* and *in vivo* [22–24,29,30], in spatial registration to printed patterns. The deposited concentrations of the signaling molecules are modulated using an “overprinting” strategy, whereby each location on a pattern is overprinted with multiple droplets of dilute bioinks, resulting in deposited concentrations increasing in direct proportion to the number of overprints.

To demonstrate that bioprinted exosomes retain the ability to signal and re-program cells similar to bioprinted growth factors, we have developed an *in vitro* model using macrophage-derived exosome bioinks printed on ECM-coated glass slides. Here, we report that bioprinted exosomes retained their spatially-defined bioactivity *in vitro*. Exosomes were isolated from three phenotypically different macrophage subsets, M0 (non-activated), M1 (pro-inflammatory) and M2 (pro-regenerative) murine macrophages. Different bioink formulations were evaluated for inkjetting reliability and exosome membrane stability during the biofabrication process. Bioprinted microenvironments were evaluated for their bioactivity by assessing their effects on C2C12 cell myogenesis.

2. Materials and methods

2.1. Cell culture

Cells were cultured in heat-inactivated fetal bovine serum (HI-FBS; Invitrogen, Carlsbad, CA) that had been depleted of exosomes. HI-FBS was ultracentrifuged at 100,000×*g* for 3 h, and the exosome depleted supernatant was aspirated (ED-HI-FBS). A macrophage cell line (J774A.1) was cultured in phenol-free RPMI medium containing 10% (v/v) ED-HI-FBS and 1% Penicillin-streptomycin (PS; Invitrogen, Carlsbad, CA). Mouse C2C12 myogenic progenitor cells (ATTC, Manassas, VA) were grown in DMEM (Invitrogen, Carlsbad, CA), 10% ED-HI-FBS and 1% PS. For M1/M2 macrophage phenotype induction, cells were treated with bacterial lipopolysaccharide (100 ng/ml; LPS; Sigma-Aldrich, St. Louis, MO) or with IL-10 (100 ng/ml; Peprotech, Rocky Hill, NJ) respectively for 72 h.

2.2. Exosome isolation

Exosomes were isolated from conditioned cell culture media of M0, M1 and M2 macrophages (72 h in cell culture) as previously described [31]. Briefly, differential centrifugation (2500×*g* for 10 min at 4 °C and 10,000×*g* for 30 min at 4 °C) was followed by ultrafiltration (0.22 μm filter; Millipore, Billicera, MA) and then size-exclusion chromatography on an Poly-Prep gravity-flow column (Bio-Rad Laboratories, Hercules, CA) packed with Sepharose 2B (Sigma-Aldrich, St. Louis, MO). The void volume fraction #4 contained the bulk of eluted exosomes. Protein concentrations of exosome fractions were determined using a BCA Protein Assay kit as recommended by the manufacturer (Pierce, Thermo Scientific, Rockford, lL). Further characterization of exosomes (see Supplemental methods) was performed using transmission electron microscopy [32,33], dynamic light scattering (DLS), tunable pulse resistive sensing (TRPS) [34,35] and western blotting [31,36].

2.3. Exosome bioink formulation

Several bioink formulations were tested to identify a bioink exhibiting jetting stability and reliability, which we defined as having a droplet velocity of greater than ~2 m/s, without satellite drop formation or nozzle clogging over a print duration of ≥1 h. The bioinks were formulated in 1X PBS with glycerol added as a humectant and to prevent agglomeration of the vesicles. The concentration of exosomes was varied from 1 to 300 μg/ml (v/v) in the following increments, 10, 50, 100, 200 and 300 μg/ml, and the glycerol concentration was varied 0–50% (v/v) in increments of 0%, 1%, 5%, 10% and 25%. The zeta-potential of various bioinks was measured using a Zetasizer (Malvern Instruments Ltd, England, UK). Exosomes diluted in PBS (1:100) were analyzed for an equilibration time of 120 s at the constant temperature of 25 °C.

2.4. Effect of inkjetting on exosome membrane integrity

The effect of inkjetting exosome bioinks on exosome membrane integrity was assessed using a previously established technique that relies on intraluminal esterase activity in exosomes [37]. Calcein Deep Red (AAT Bioquest Inc, Sunnyvale, CA) was solubilized in DMSO and diluted with 1X PBS to a final concentration of 10 μM. Exosomes were isolated and labeled with Calcein Deep Red prior to subjecting them to sonication (10 min continuous pulse at 60% amplitude using a 0.25″ tip using Fisher brand model 505 Sonic membrator) or inkjet deposited using the inkjet in the bioprinter described below. Native exosomes were used as a positive control. CD63-conjugated magnetic beads (ExoCap, MBL International, Woburn, MA) were prepared as previously described [32]. Briefly, monoclonal anti-CD63 antibody (MA5–24169, Invitrogen, Carlsbad, CA) was biotinylated using a one-step antibody biotinylation kit purchased from Miltenyi Biotec (Auburn, CA) as recommended by the manufacturer. Biotinylated CD63 antibody (5 μg) was incubated with thoroughly washed 0.5 ml of streptavidin coated magnetic beads (1×10^8 beads/ml) for 1 h at 25 °C under constant agitation. 1 μg of non-printed exosomes, bioprinted exosomes and sonicated exosomes were each incubated with 100 μl of CD63-conjugated magnetic beads for 16 h at 4 °C under constant agitation. To assess membrane integrity, exosomes were captured on CD63 magnetic beads, washed x3 with PBS and 20,000 events/treatment were

analyzed on Accuri C6 flow cytometer (BD Biosciences, San Jose, CA) connected to an Intellicyt HyperCyt autosampler (IntelliCyt Corp., Albuquerque, NM) using Cy5 channel (649 nm). Data were processed and interpreted using FlowJo ® software (FlowJo LLC, Ashland, Oregon).

2.5. Bioprinting

Bioprinting of exosomes was accomplished using our previously described custom inkjet-based system [23,24,30,38–41], which has since been updated with several features, including integration of: 1) a JetXpert™ a drop-in-flight analysis system (ImageXpert, Inc., Nashua, NH) to evaluate jetted droplet formation and jetting stability; 2) Polypropylene filters (1000 µl Neptune pipette filters, Biotix incorporated, CA) in the inkjet vacuum lines to trap any exosomes that might inadvertently get sucked up into those lines; 3) a highly localized exhaust snorkel around the jetting area to further protect operator exposure from the remote possibility of exosome aerosolization; and 4) new bioink reservoirs system (see Fig. 2A). The inkjet used for these studies was a piezoelectric drop-on-demand printhead with a 60 µm diameter nozzle (unless otherwise noted) with a diamond-like coating to mitigate tip wetting (MicroFab Technologies, Inc., Plano, TX). Although higher resolutions are achievable using smaller diameter nozzles, there is a trade-off between jetting reliability and resolution, *i.e.,* the smaller the nozzle, the smaller the drops, but the more prone to nozzle clogging. Prior to printing, the printhead was sterilized by first rinsing with 70% ethanol followed by three rinses with sterile (0.2 µm of filtered) deionized water. Inkjetting was performed using a biopolar waveform: 25 µsec dwell at +12 V and 40 µsec echo at −12 V. Jetting of final patterns was performed on-the-fly using a table speed of 0.5 mm/sec and drop spacing of 80 µm, resulting in a jet firing rate of 6.25 Hz. These parameters were also used for the stationary jetting described above to access membrane integrity.

Prior to loading the bioink into the jet, the inner surface of the glass capillary tube component of the jet was absorbed with 1% bovine serum albumin (0.2 µm filtered) for 15 min at 25 °C to minimize non-specific binding of exosomes to the ink reservoir tube. Small volumes of bioinks (~30–45 µl) were then loaded into the jets using a 'dip & sip' approach whereby the jet tip is lowered into a ~ 100 µl aliquot on a parafilm tape (Bemis NA, Neenah, WI) and then a small vacuum was used to suck the liquid up into the jet. The larger glass reservoirs seen in Fig. 2A are used to hold distilled water and isopropyl alcohol for jet cleaning.

The deposited concentrations of exosomes on ECM substrates were modulated using an overprinting strategy as previously described [42,43], where 'OP' (referred to in sections below) signifies the number of overprints (OPs) of dilute bioinks deposited at each substrate location to modulate delivered bioink dosage. If the time between depositing droplets on a given location is too short, then large puddles form until the droplets dry. To mitigate puddling, we use a printing strategy that over prints in a layer-wise fashion, *i.e.* one drop per layer per pixel to increase the time between drop depositions at each location. Furthermore, if the time between printing two adjacent locations ('pixels') is too short, a drop drying on one location can coalesce with the adjacent drop, thus forming a puddle. Therefore, we print each layer in two passes whereby every other pixel location in one sub-layer is printed, and then the remaining pixels are printed in the next sublayer. The overprinting strategy was validated by creating concentration gradients.

2.6. ECM substrates

The ECM printing substrate for *in vitro* experiments was selected by first testing various ECM-coated coverslips for exosome binding capacity using PKH26 labeled exosomes. The ECMs tested included fibrinogen (Enzyme Research Laboratories, South Bend, IN), fibrinogen (Enzyme Research Laboratories, South Bend, IN), basement membrane extract (Trivigen, Gaithersburgh, MD), BSA (Sigma-Aldrich, St. Louis, MO), laminin (Sigma-Aldrich, St. Louis, MO), collagen type I (Sigma-Aldrich, St. Louis, MO), vitronectin (Sigma-Aldrich, St. Louis, MO), fibronectin (Sigma-Aldrich, St. Louis, MO), collagen type IV (Sigma-Aldrich, St. Louis, MO), poly-L-Lysine (Sigma-Aldrich, St. Louis, MO), and, no coating (control). The ECM-coated coverslips were prepared according to previously described protocol [21,29,42]. Retention of printed exosome patterns on ECM-coated coverslips was evaluated using PKH26 labeled exosomes. *In vitro* cell culture retention studies were performed by incubating the bioprinted coverslips in simulated body fluid (DMEM, 10% FBS, 25 mM HEPES, 0.1% sodium azide) for designated timepoints in a regular cell culture incubator (37 °C, 5% CO_2 and 95% relative humidity) and measuring the exosome fluorescence intensities postwashing with PBS.

2.7. Internalization of solid-phase exosomes

PKH26-labeled exosomes were printed as a 500 µm × 500 µm pattern with 50 OPs (47 ng total exosome protein per pattern) followed by overnight rinsing in 1X PBS prior to seeding of C2C12 cells (P2-P6). C2C12 cells were grown and maintained in DMEM media supplemented with 10% FBS. At designated timepoints, cells were treated with acid stripping buffer (500 µM NaCl and 0.5% acetic acid in DI water), pH 3.0 for 45 s followed by three washes with 1X PBS to remove plasma membrane-bound exosomes. Cells were fixed with 1.6% freshly prepared paraformaldehyde (Electron Microscopy Services, Hatfield, PA) for 20 min at 25 °C. Excess fixative was quenched by adding an equal volume of 1% (w/w) BSA in PBS for 5 min followed by three washes with 1X PBS. To study immobilized exosome uptake, cells were seeded on bioprinted microenvironments for designated timepoints prior to fixation. Fixed cells were permeabilized with 0.1% TritonX 100 in PBS for 1 min. To visualize F-actin and nuclei, cells were stained with Alexafluor488-Phallodin (Thermo Fisher Scientific, Waltham, MA) (5:200 in 1X PBS) and Hoechst 33342 (Thermo Fisher Scientific, Waltham, MA) (1:1000 in 1X PBS), respectively. Imaging was performed using a Carl Zeiss LSM 880 confocal microscope with fixed settings across all the experimental time points and the images were analyzed using ZEN Black software (Carl Zeiss Microscopy, Thornwood, NY). Solid-phase exosome internalization was also studied using flow cytometry. Briefly, 3 patterns (0.5 mm × 0.5 mm, 1 mm x 1 mm and 1.5 mm × 1.5 mm) of PKH67 labeled exosomes representing increasing OPs (10, 20 and 40 OPs, respectively) were printed on collagen type-1 coated coverslips and seeded with C2C12s for 24 h at a density of 5000 cells/mm^2. Cells on the entire coverslip were trypsinized and assessed for exosome uptake on Accuri C6 flow cytometer (BD Biosciences, San Jose, CA) connected to an Intellicyt HyperCyt autosampler (IntelliCyt Corp., Albuquerque, NM) using FITC channel.

2.8. Raw Blue assay

RAW-Blue™ cells (murine RAW 264.7 macrophage reporter cell line) were purchased from InvivoGen (San Diego, CA). This reporter cell line stably expresses a secreted embryonic alkaline phosphatase (SEAP) gene inducible by NF-kB activation that can be detected calorimetrically. RAW-blue cells were grown and maintained in high-glucose DMEM supplemented with 10% HI-FBS, 1% PS and 100 µg/ml Normicin™ (Invivogen, San Diego, CA) and were used between passages 3–7 for all the experiments described. The assay was performed according to manufacturer's instructions. Briefly, 20,000 RAW-blue cells and treatments consisting of 10 µg/ml M0, M1, M2 exosomes or 100 ng/ml LPS (positive control) were added to 96 well plates in triplicate and incubated for 24 h under culture conditions (37 °C, 5% CO_2 and 95% relative humidity). Post incubation, 20 µl of conditioned media was collected and incubated with 200 µl QUANTI-blue™ reagent (Invivogen, San Diego, CA) and optical density at

655 nm was measured using TECAN spectrophotometer (TECAN, Männedorf, Switzerland).

2.9. Proliferation assay

Proliferation was quantified by using a direct CyQUANT nucleic acid-sensitive fluorescence assay (Thermo Fisher Scientific, Waltham, MA, USA) according to the manufacturer's instructions. Briefly, 200 µl aliquots of cell suspension containing 1.3×10^3 C2C12 cells/ml were plated in wells of a 96-well microplate (Corning Inc., Corning, NY, USA) and allowed to adhere for 6 h. Exosomes (10 µg/ml) from M0, M1 or M2 macrophages were added to respective treatment wells for 72 h. An equal volume of PBS was added to the control group (no treatment). Cells were then labeled with CyQUANT® Direct and fluorescence intensities were measured with TECAN spectrophotometer reader (TECAN, Männedorf, Switzerland). Proliferation was assessed by plotting relative fluorescence intensities across different treatments and under two different conditions – 10% FBS (growth media) and 2% FBS (myogenic differentiation media).

2.10. Myogenesis assay

C2C12 stem cells were grown to 80–90% confluence and induced to differentiate into myoblasts in the presence or absence of both liquid-phase and solid-phase exosomes. Expression of a skeletal muscle differentiation marker myosin heavy chain II (MF20) was assessed by immunostaining and quantified by analyzing the fusion index. For solid-phase myogenic differentiation, 1.75 × 1.25 mm patterns at 50 OPs (76 ng of total exosome protein per pattern) were printed, rinsed overnight in 1X PBS and C2C12s were seeded. Post adherence, growth media (supplemented with 10% FBS) was changed to differentiating media (2% FBS) and cells were allowed to differentiate for 48 h prior to fixation.

2.11. Immunofluorescence staining

Post treatment cells were washed in 1X PBS, fixed in 3.33% paraformaldehyde (PFA; Electron Microscopy Services, Hatfield, PA) for 20 min at room temperature and permeabilized with 0.1% TritonX 100 (Millipore-Sigma, St. Louis, MO) for 10 min. To minimize non-specific binding, blocking was performed with 10% goat serum for 20 min at RT. Cells were then rinsed with wash buffer (PBS, 0.1%BSA) and incubated with 1:100 dilution (PBS with 0.1% BSA) of primary antibodies rabbit anti-mouse MF20 (MAB4470, R & D Bio-Techne Corporation, Minneapolis, MN) overnight at 4 °C. Cells were then rinsed 3X with wash buffer and incubated with 1:500 (PBS, 1% BSA) dilution of secondary antibody goat anti-mouse Dylight 488 nm (4408S, Cell Signaling Technologies, Denvers, MA) for 2 h at 25 °C. Lastly, cells were rinsed x5 with 25 °C wash buffer and imaged using a Zeiss LSM 880 confocal microscope (Carl Zeiss, Thornwood, NY). For liquid-phase experiments, fluorescence was quantified by imaging 3 equally spaced field of views (FOVs), with a FOV (1.32 mm by 1.80 mm) corresponding to Carl Zeiss objective (5X magnification, 0.16 NA). The intensity of fluorescence in the FOV was measured using image J software (NIH, Bethesda, MD) post background correction. Myotube fusion index (MFI) was quantified by manually measuring the percentage of nuclei in myotubes in the FOV defined above. For solid-phase experiments, quantification of MF-20 expression was performed as previously described [22]. Briefly, the rectangular marquee tool was used to draw a region of interest (ROI) on-pattern and off-pattern corresponding to half of the bioprinted pattern (representing an area 0.875 mm by 0.625 mm in size). Quantitation of ROIs was performed using Image J software post background correction. Solid-phase MFI was quantified within the same ROI by manually counting the percentage of nuclei in myotubes.

2.12. Statistics

For statistical analysis, all data was subjected to Analysis of Variance (ANOVA) followed by Tukey's Post Hoc test for multiple comparisons between treatment groups and their controls using Systat (SYSTAT Software, Inc., Chicago, IL). Statistical significance was defined at $p \leq 0.05$. All the experiments were performed a minimum of two times with replicates of 2 or 3.

3. Results

3.1. Exosome isolation and characterization

The average size of isolated exosomes was approximately 100 nm as determined by DLS and TRPS (Supplemental Fig. 1A and B), and the protein concentration was 100–160 µg/ml depending on the source

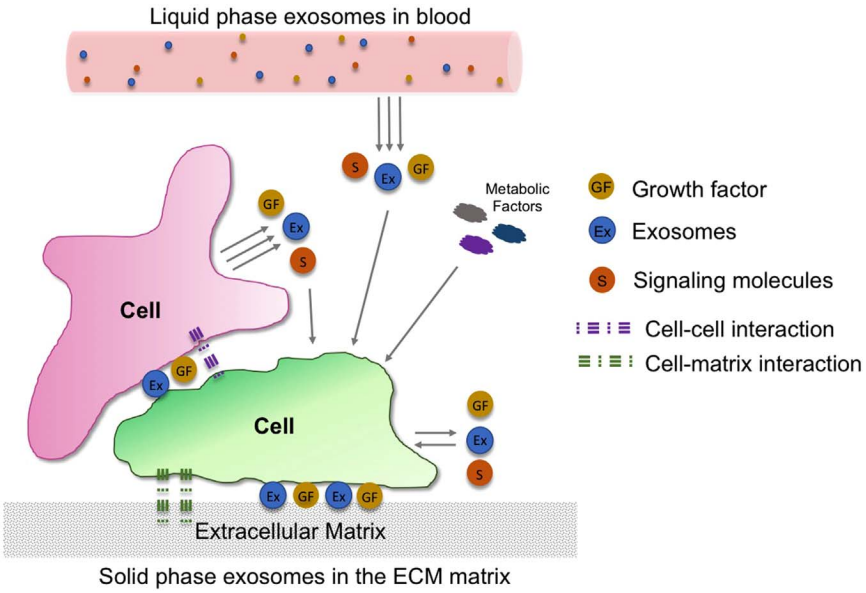

Fig. 1. Schematic showing exosomes present in the tissue microenvironment. Similar to growth factors, exosomes occur both in a 'liquid-phase' suspended in body fluids and in a 'solid-phase' immobilized *via* native binding affinities to the extracellular matrix (ECM).

and passage number of the cell line harvested. Transmission electron microscopy (TEM) showed the presence of vesicles around 100 nm in size, confirming they are exosomes rather than microvesicles. Exosomes were also assessed for the presence of tumor susceptibility gene 101 protein (TSG101), a specific endoxomal sorting complex marker, and for CD63 and CD9 as shown in Supplemental Fig. 1C. Collectively these characteristics are typically indicative of the exosome subpopulation of EVs. However we also recognize that other EV subpopulations may also exist within our 'exosome' isolates.

3.2. Exosome bioink formulation

Increasing the concentration of glycerol in bioinks resulted in a decrease in the zeta potential of the bioink as shown in Fig. 2B. Moreover, increasing the glycerol concentration decreased the droplet velocity and droplet volume as shown in Fig. 2C and D. A reliable exosome bioink formulation was determined to be 10 µg/ml exosomes with 10% glycerol in PBS buffer. Even though higher concentrations of exosomes exhibited reliable jetting, the more dilute formulation was chosen to permit finer resolution over the number of OPs that could be printed. For example, 25% glycerol resulted in coalescing of deposited drops as shown in Supplemental Fig. 2. Based on our prior experience, reliable jetting was defined as generation of stable droplet with a speed of > 2 m/s without satellite drop formation. While lower concentrations of viscous glycerol produced velocities > 2 m/s, the inkjet nozzle was more prone to clogging due to evaporation of water at the nozzle tip, leading to locally high ink concentrations at the tip. Hence, as a trade-off between droplet velocity and nozzle clogging, 10% glycerol was chosen to achieve suitable jetting over lengthy print durations (≥1 h print time).

The effect of bioprinting on exosome membrane integrity was assessed using on-bead flow cytometry as shown in Fig. 1E. There was no difference between native and bioprinted exosomes, suggesting that physical forces during inkjet-based bioprinting have minimal effect on exosome membrane integrity.

Coverslips coated with 100 µg/ml collagen type-1 were selected for the *in vitro* studies based on its high exosome binding capacity (Fig. 3A).

The 60 µm inkjet produced approximately 70 ± 4.87 pl droplets with 1.8 ± 0.52 m/s velocity, yielding approximately 75 µm diameter deposited splat. The variation in droplet volume can be attributed to environmental conditions such as humidity. Patterns of concentration modulated arrays of PKH26 labeled exosomes, each measuring 0.5 mm × 0.5 mm, were created on collagen type-1 coated coverslips as shown in Fig. 3B. The patterns shown in Fig. 3B consisted of 80 µm spacing between individual deposited droplets. To study the effects of nozzle diameter on deposited drop diameter, a combinatorial array was printed using a dual-inkjet set up (60 µm and 30 µm) as shown in Fig. 3C.

All the solid-phase cell culture experiments were performed with a drop spacing of 80 µm resulting in close packed splats within patterns. Printed patterns of M1 and M2 exosomes persisted up to 96 h under cell culture conditions on collagen type-1 coated coverslips as shown in Fig. 3D.

3.3. Solid-phase exosomes are available for cellular uptake

PKH26-labeled solid-phase exosomes were internalized by C2C12 cells starting as early as 15 min as shown in Fig. 4A. With increasing

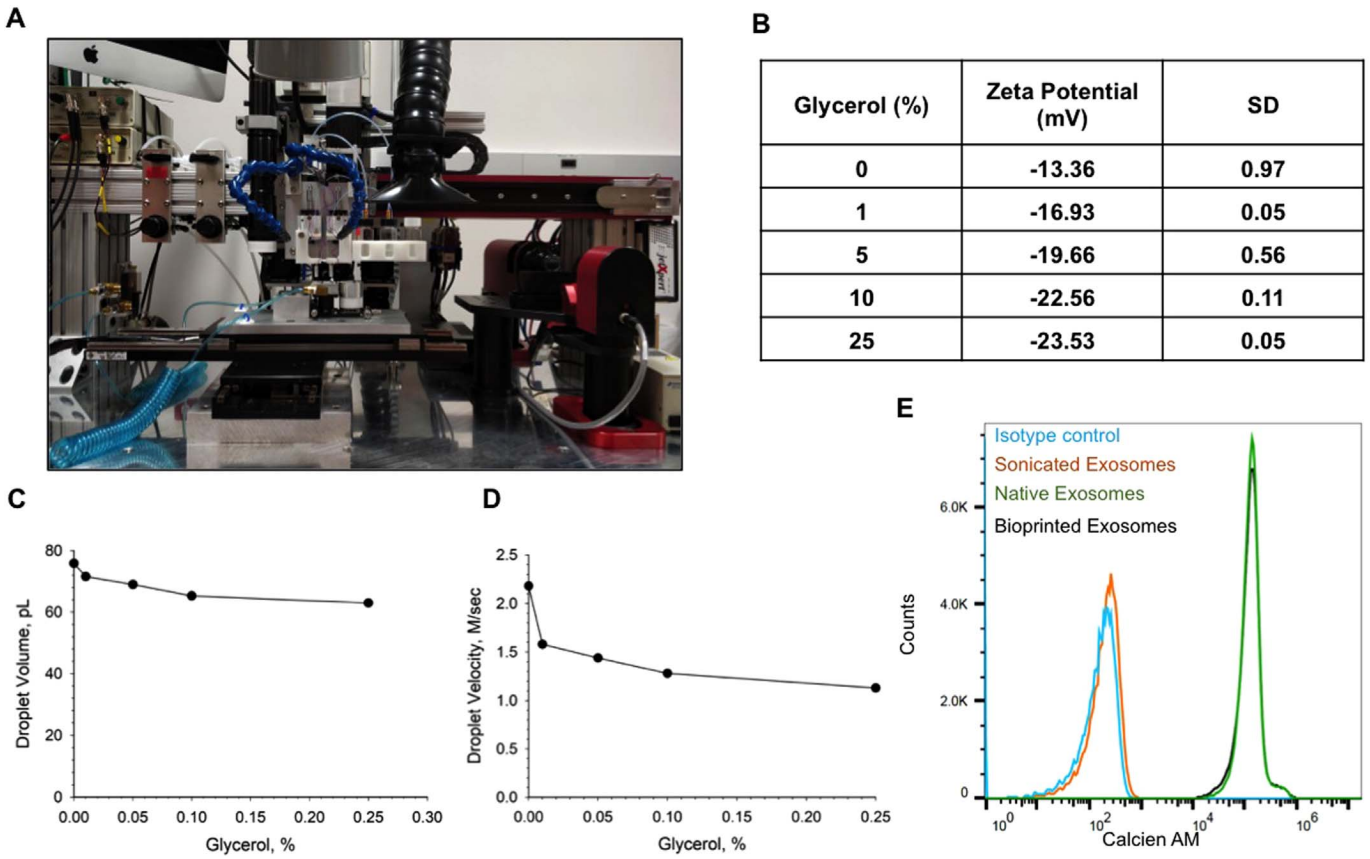

Fig. 2. Exosome ink formulation and bioprinting. (A) Photograph of custom inkjet- bioprinter. (B) Zeta-potential values of various exosome-bioink formulations. (C) Droplet volume of different exosome-ink formulations. Plots indicate mean ± SEM (n = 3 experiments) (D) Droplet velocity of different exosome-ink formulations. Plots indicate mean ± SEM (n = 3 experiments) (E) On-bead flow cytometry histograms showing exosome-membrane stability during the bioprinting process. Histograms represent 100,000 events. Sonicated exosomes lost the calcein AM signal, whereas bioprinted exosomes showed no significant change in the fluorescence intensity from the calcein AM dye as compared to native exosomes.

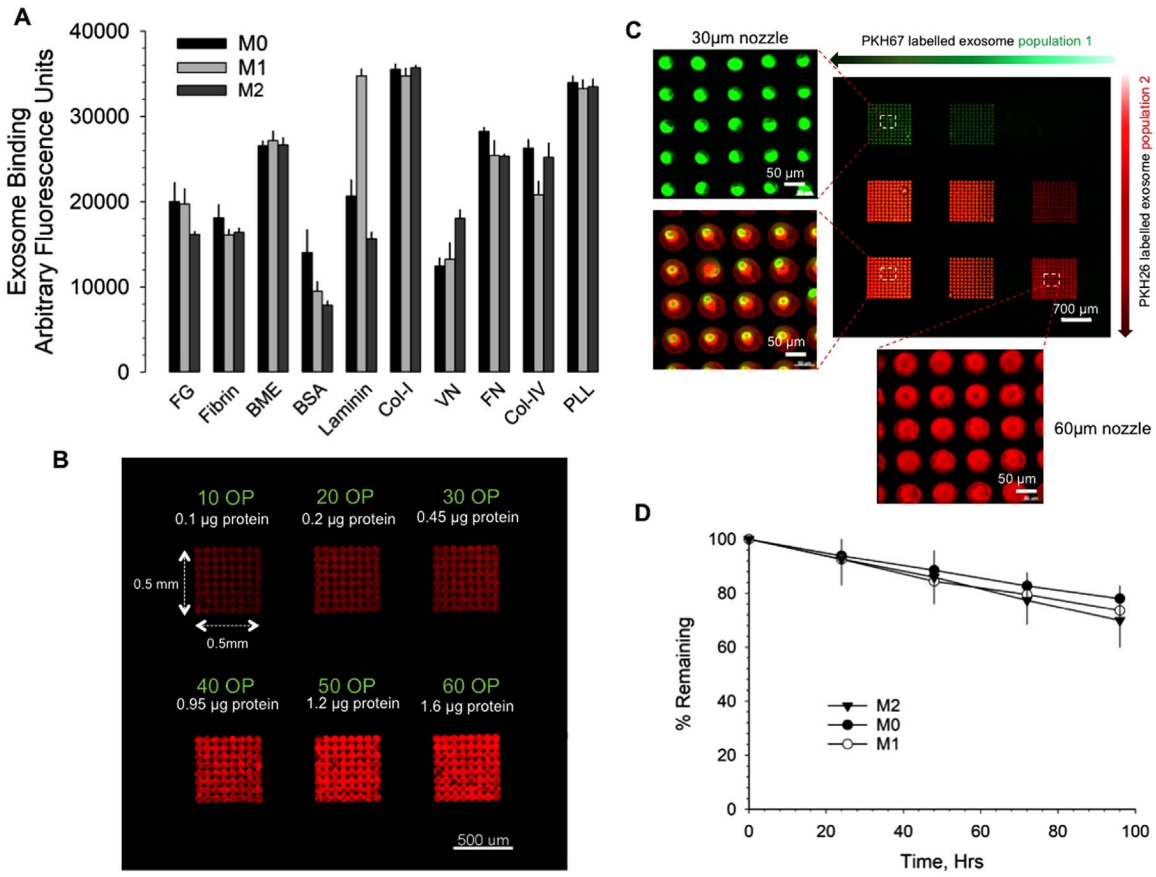

Fig. 3. (A) Binding efficiency of PKH26 labeled exosomes to different ECM-coated coverslips. Bars indicate mean ± SEM (n = 3 experiments). (B) Overprint modulation of exosome microenvironments on collagen type-1 coated coverslips. The 60 µm inkjet produced approximately 75 µm diameter deposited spots. (C) Combinatorial array of two different populations of exosomes demonstrating the control over deposited drop resolution. The PKH67 (pseudo green)-labeled exosomes were printed from a 30 µm nozzle with 100 µm spacing resulting in a splat diameter of 40 µm whereas the PKH26 (pseudo red)-labeled exosomes were printed using a 60 µm nozzle with 100 µm spacing resulting in a 75 µm spat diameter. (D) Persistence of exosome patterns in *in vitro* conditions up to 4-days. Bars indicate mean ± SEM (n = 3 experiments).

time, the internalized exosomes appeared to localize around the perinuclear region. Cellular uptake of solid-phase exosomes was confirmed with 3D confocal Z-stacking (Supplemental video 1) and flow cytometry (Fig. 4B).

Supplementary material related to this article can be found online at doi:10.1016/j.bprint.2019.e00041.

3.4. M1 exosomes induce NF-kB expression in RAW 264.7 macrophages

M0 and M2 exosomes did not induce NF-kB expression in RAW-blue cells as shown in Fig. 5B compared to the control. Whereas M1 exosomes induced significant upregulation of NF-kB expression compared to the control suggesting the presence of pro-inflammatory signaling agents.

3.5. Effect of liquid-phase M0, M1 and M2 exosomes on C2C12 proliferation

Under growth conditions, all the three exosome populations (M0-, M1- and M2-derived) increased the rate of proliferation in C2C12 cells. Under differentiation conditions, only M1 derived exosomes increased their proliferation as compared to controls (Fig. 5C and Supplemental Fig. 3). M0 and M2 exosomes did not have any significant effect on proliferation of C2C12 cells under differentiation conditions compared to controls.

3.6. Effect of liquid-phase M0, M1 and M2 exosomes on C2C12 cell differentiation

Myogenesis is the default differentiation lineage when C2C12 culture serum is reduced as evidenced by formation of myotubes and upregulation of myosin heavy chain (MF20) expression [22]. Liquid-phase M1 exosomes significantly lowered the number of myotubes and MF20 expression compared to the control group, whereas M2 exosomes upregulated myogenic differentiation (Fig. 5D and E). M0 exosomes resulted in a dose-dependent increase in C2C12 cell differentiation. M2 exosomes increased the myotube fusion index significantly more than M0 exosomes, whereas M1 exosomes inhibited myotube fusion as shown in Fig. 5F.

3.7. Effect of solid-phase M1 and M2 exosomes on C2C12 differentiation

The myotube formation was inhibited in C2C12 cells cultured on the patterns of printed M1 exosomes. MF20 expression was significantly lower for all M1 printed dose patterns compared to both M0 and M2 groups (Fig. 6C). Whereas M2 at 10 OPs was less than M0 at 10 OPs, M2 was greater than M0 at other printed doses. M0 at 40 OPs was greater than the lower M0 doses. Alternatively, C2C12 cells cultured on patterns of printed M2 exosomes promoted myogenic differentiation as evidenced by increased myotubes and expression levels of MF20 in registration to the printed M2 patterns. The MFI values indicated a significant dose response for M2 over M0 at all printed doses whereas M1 exosomes inhibited the MFI response compared to both M0 and

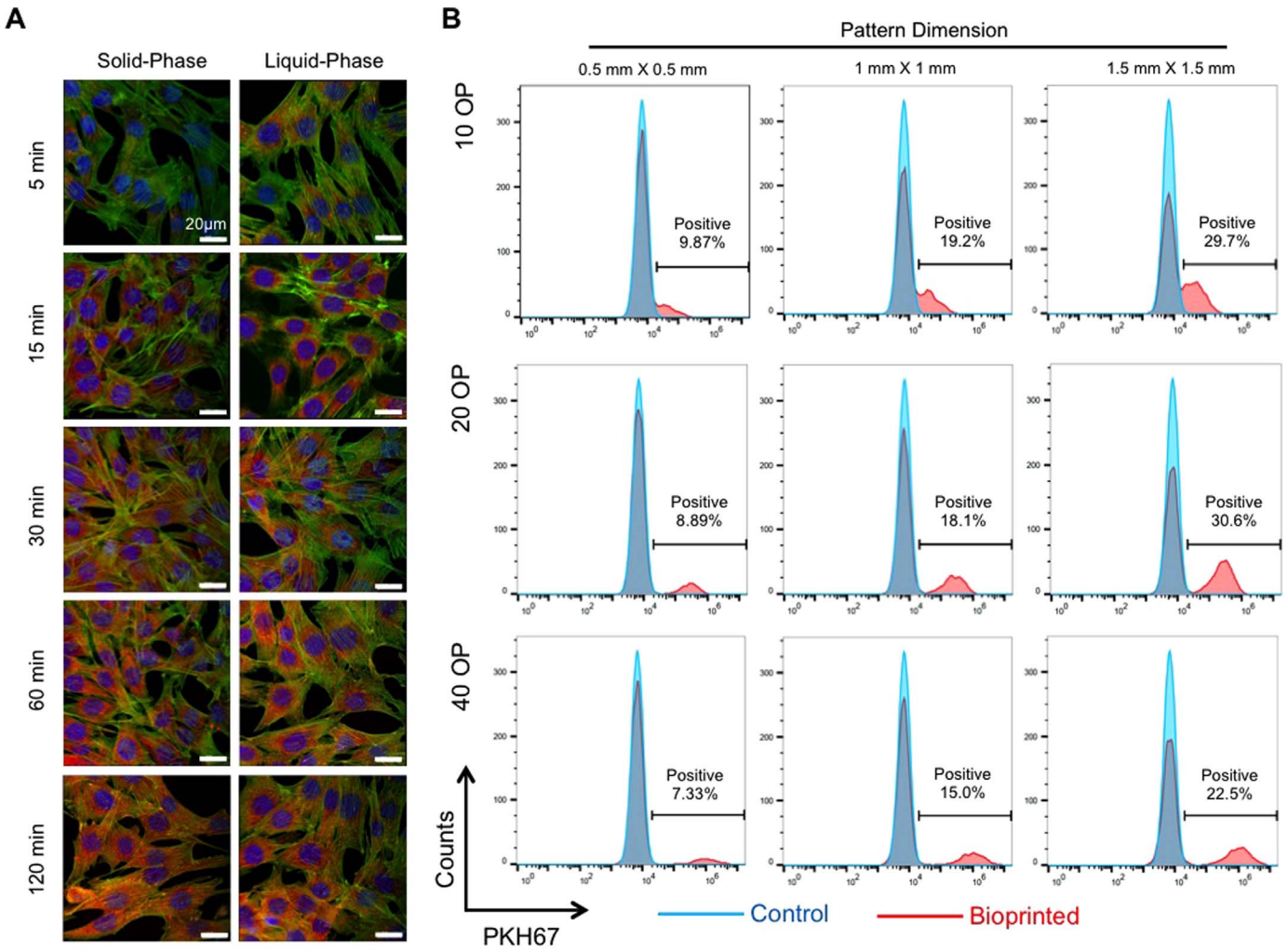

Fig. 4. Exosome internalization studies (A) Representative confocal micrographs showing time-dependent uptake of liquid-phase and solid-phase exosomes. Nuclei (blue), F-actin (green) and exosomes (red), Scale bar = 20 μm. (B) Representative flow cytometry histograms showing uptake of solid-phase M0-exosomes by C2C12 cells in a concentration and pattern-dependent manner. Increasing overprints resulted in increased fluorescence intensity and pattern dimensions led to increase in cell counts with internalized exosomes. Histograms represent 20,000 events per treatment or control group within a single experiment. Two independent experiments were performed with similar results.

M2 at all printed doses (Fig. 6D). A patterned differentiative response was visible by eye within tissue culture wells, as shown by the scanned images of the culture wells in Fig. 6. An increased magnification of the tissue culture wells demonstrated the dose-dependent pattern response to cells on the M2 patterns (Fig. 7). C2C12 differentiation was dose-dependent on the surface concentration of printed M2 exosomes, with the highest surface concentration inducing differentiation of cells located on the region in registeration to printed pattern that corresponds to the M2 exosome array, whereas cells outside the spatially defined M2 exosome pattern exhibit appreciably lower number of myotubes and less MF20 expression. The intense nuclear staining on 40 OPs of the M2 exosome pattern could be attributed to excess staining artifact due to the high number of nuclei on-pattern. Together, these data suggest a regulatory role for solid-phase exosomes in the myogenesis.

4. Discussion

Here, we demonstrate for the first time highly controlled inkjet-based biofabrication of well-defined exosome microenvironments that are biologically active, impacting cell behavior in a spatially controlled manner. The stability of exosomes during the bioprinting process was validated and the resulting bioprinted microenvironments were assessed for deposited concentrations (validation of overprinting strategy) and the patterns persistence under simulated *in vivo* conditions. Bioactivity of bioprinted microenvironments and spatial control over cell responses was confirmed by utilizing exosomes isolated from different macrophage subsets (M0, M1 and M2) and by determining their effects on C2C12 cell myogenesis. Given that the main focus of our group has been on musculoskeletal tissue regeneration, we used macrophage-derived exosomes as a paradigm source, because differentially stimulated macrophages have been reported to regulate myogenesis both *in vitro* and *in vivo* [44–49].

In contrast to soluble exosomes, exosome biological activity as ECM bound solid-phase constituents remains underexplored. Matrix vesicles and matrix-bound nanovesicles were originally identified and isolated from tissue ECMs [50–52]. Decades of work have focused on matrix vesicles and their physical interaction with the ECM, especially with collagen [53], and their role in regulating biomineralization under normal and pathophysiological conditions [54]. Recent identification of biologically active matrix-bound nanovesicles associated with a range of soft tissues broadens the significance of potential tissue-specific ECM immobilized exosomes [52,55]. Therefore, it is of paramount importance to be able to engineer solid-phase exosome microenvironments to study their biology and to ultimately translate such ECM-exosome interactions to the localized delivery of exosome-based therapeutics in the future, minimizing total delivered exosome dosage while limiting off-target effects.

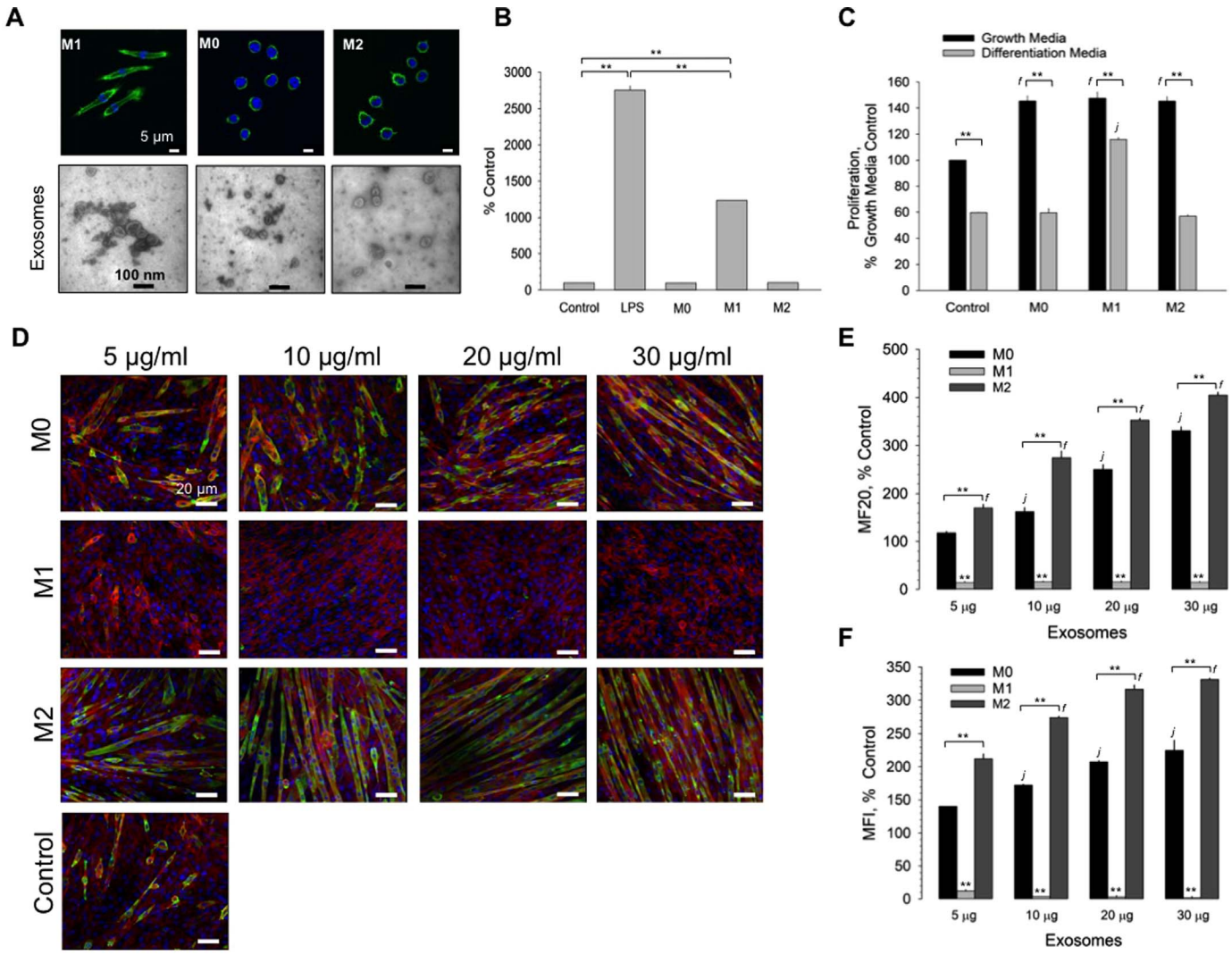

Fig. 5. Effect of liquid-phase macrophage-derived exosomes on C2C12 myoblast differentiation. (A) Representative confocal micrographs (scale bar = 5 μm) and transmission electron micrographs (scale bar = 100 nm) corresponding to M0, M1 and M2 phenotypes. F-actin (green) and Nuclei (blue). (B) RAW-blue reporter assay showing induction of NF-kB expression as a result of exposure to exosomes from M0-, M1 and M2 macrophages. Bars indicate mean ± SEM (n = 3 experiments). (C) CyQUANT proliferation assay showing effect of M0, M1 and M2 exosomes on C2C12 proliferation at 72 h post treatment under growth (10% FBS) and differentiation (2% FBS) conditions. Bars indicate mean ± SEM (n = 3 experiments). (D) Representative confocal micrographs of C2C12s treated with increasing doses of M0, M1 and M2 exosomes immunostained for F-actin (red), Nuclei (blue), MF20 (green). Scale bar = 20 μm (E) Quantification of MF20 quantification of C2C12s treated for 48 h with different dosages exosomes from M0, M1 and M2 macrophage phenotypes. MF20 staining intensity was adjusted for corresponding nuclear staining intensity and reported as % non-treatment control. Bars indicate mean ± SEM (n = 3 experiments) (**F**) Quantification of myotube fusion index. Bars indicate mean ± SEM (n = 3 experiments). * *, represents $p < 0.01$, *f* and *j* represent $p < 0.05$ difference compared to their respective control groups or to M0 groups.

In addition to inkjetting, there are several biopatterning processes to consider that could be adapted to engineer defined exosome microenvironments. These alternative processes, however, have limitations in addressing our specific requirements, including: low volume of prototype bioinks; programmable patterning and dose control; non-contact; use of native binding affinities to immobilize exosomes to native substrates for biomimicry of the solid-phase; and, translatable to *in vivo* studies. For example, microfluidics technology [56] could be applied to dynamically control both spatial and temporal *in vitro* delivery of exosomes, however, it is not clear how such an approach would practically translate *in vivo*. Photolithography, photoimmobilization [57–59], soft lithography and microcontact printing [60] use either non-physiological substrates (scaffolds) and/or would require chemical modification of the printed exosomes to achieve immobilization. They also require custom manufacture of masks for each different pattern, which is time and labor intensive. Precision aerosol-based spraying [56] is a versatile approach that does not require a custom manufactured mask or contact with the substrate, and pattern designs can be easily changed with CAD/CAM programing; however, this deposition approach currently requires a relatively large reservoir of ink (approximately 1 ml) to create the aerosol, which can be cost and preparation time prohibitive for prototyping constructs with exosome bioinks. One possible issue with inkjet printing is its resolution, which is typically 20–50 pl drops that spread out as 50–100 μm splats when jetted on planar substrates, and therefore not able to create sub-micron feature sizes like microcontact printing or photolithography. However, we and others have found inkjet-based protein patterning resolution to be sufficient to spatially drive desired cell responses both *in vitro* [20,40] and *in vivo* [39,61].

For inkjet printing, formulation of functional inks is a balance between having suitable fluid properties to allow stable droplet formation, reliable clog-free printing, and are compatible with over printing multiple drops at the same 'pixel' location. One of the major hurdles with printing particulate-based suspension inks is sedimentation and/agglomeration of particles in the inkjet during the printing process [62]. Sedimentation is not a concern with exosomes as they are relatively small (approximately 100 nm in diameter). However, agglomeration and clumping due to non-specific surface protein-protein

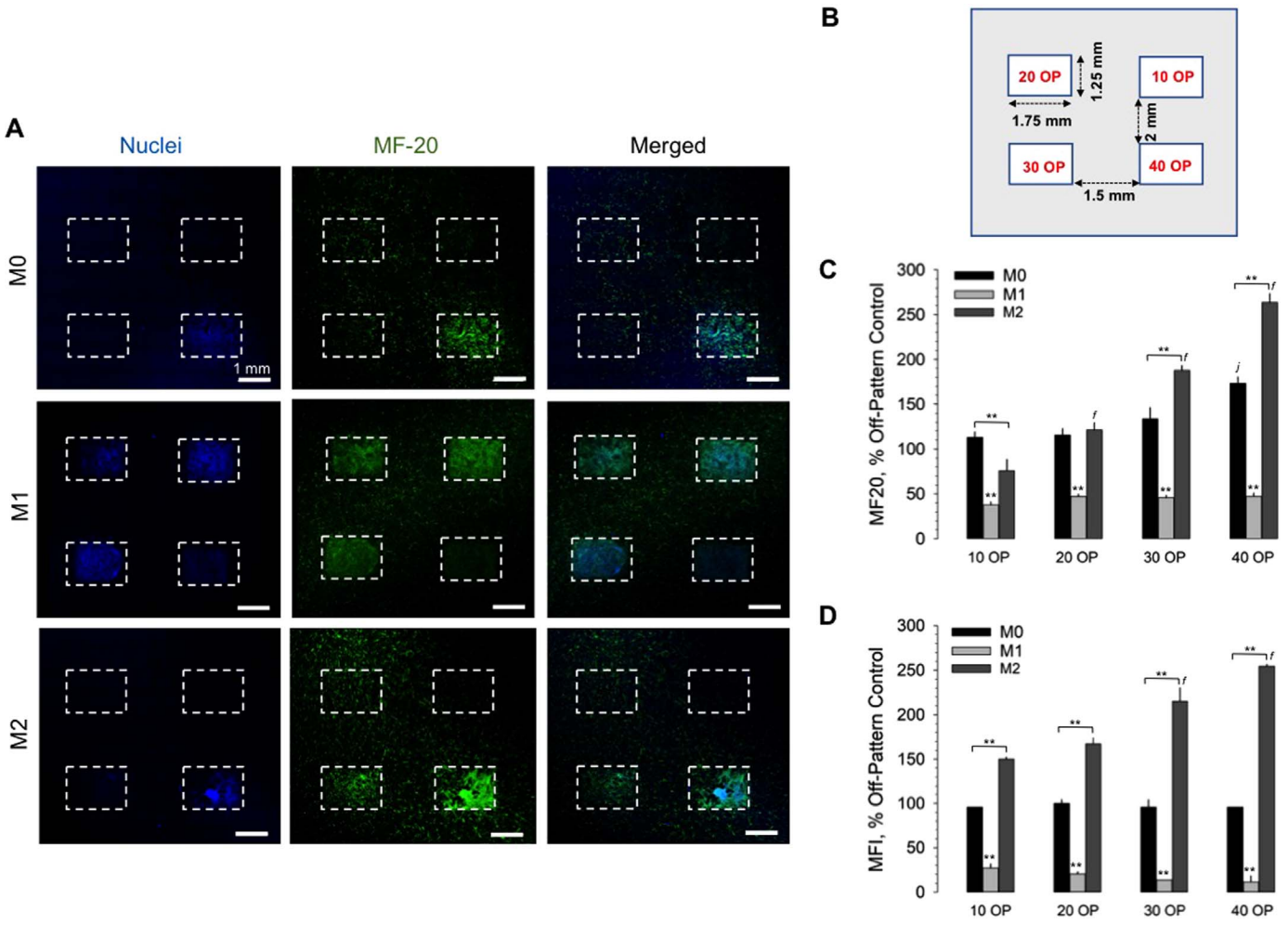

Fig. 6. Effect of solid-phase macrophage-derived exosomes on C2C12 myogenesis. (A) Representative confocal tiled-micrograph showing dosage curve of solid-phase M0, M1 and M2 exosomes. Nuclei (blue) and MF20 (green). Scale bar = 1 mm. (B) Schematic showing bioprinted microenvironments consisting of varying OPs of 1.75 mm × 1.25 mm patterns. (C) Quantification of MF20 fluorescence intensity on- and off-patterns. MF20 staining intensity was normalized to corresponding nuclear staining intensity within the field of view accounting for differential proliferative effects of macrophage exosomes and reported as % off-pattern control. Bars indicate mean ± SEM (n = 2 experiments). Quantification of myotube fusion index on- and off-patterns. Bars indicate mean ± SEM (n = 2 experiments). **, represents $p < 0.01$, *f* and *j* represent $p < 0.05$ difference compared to their respective control groups or to M0 groups.

interactions between exosomes can cause issues during the printing process. To avoid this, glycerol was used as an additive, which not only increases the viscosity on the bioink, reducing the exosome agglomeration rate, but it also acts as a humectant reducing the evaporation of the solvent at the nozzle tip. Moreover, zeta-potential studies indicate that increasing the concentration of glycerol made the zeta-potential more negative, which could potentially mitigate agglomeration and clumping of exosomes. In contrast, a high concentration of glycerol can result in a number of problems. When printed drops impact the printing substrate, the liquid evaporates leaving behind the exosomes and the buffer salt. If one drop is deposited on top of another prior to the first drop drying, a puddle of solvent can build-up and exosomes can spillover to adjacent pixels in an uncontrolled fashion. Drop drying times are on the order milliseconds when there are no additives involved. However, glycerol can reduce the evaporation rate in a substantial manner when droplets are being deposited on a minimally absorbing substrate, such as a thin coating of ECM on a glass-coverslip, resulting in formation of 'puddles' of deposited droplets effecting the overall geometry of the pattern as seen in Supplemental Fig. 2. We found that 10% glycerol is sufficient to prevent agglomeration of exosomes while permitting for effective use of the overprinting strategy. Though higher concentrations of glycerol permitted use of higher concentrations of exosomes (up to 300 μg/ml) in the ink, it also affected the wet-dry cycles between overprinted deposited droplets, resulting in coalescing of consecutive drops forming a 'puddle' (Supplemental Fig. 2). The bioinks were normalized to protein concentration rather than vesicle counts as this is a common practice in extracellular vesicle-related research [63,64].

We employed light microscopy and immunostaining to determine spatial cell responses to exosome patterns. Light microscopy dictates that we use very thin constructs. Therefore, for these applications we used relatively thin layers (10 s of nanometers) of ECM materials, such as collagen type-1, coated on and cross-linked to glass cover-slips using epoxy-silane chemistry [42]. However, using collagen as the ECM component of the exosome microenvironment could be translated to the fabrication of much thicker 3D implantable exosome/collagen constructs for future *in vivo* studies. We previously reported on biopatterning of growth factor bioinks on FDA-approved sheets of native ECM scaffolds, such as 200 μm thick human acellular allografts, where the printed inks absorbed into and bound to the ECM, and then implanted these constructs to demonstrate biopatterning *in vivo* [39,61,65]. It follows that ECM scaffold sheets, which are currently used in the clinic [66], could similarly be biopatterned with exosome bioinks for *in vivo* applications. Individual layers of these native ECM materials are sufficiently thick for use in small animal models, however, if needed, larger-scale and/or more complex-shaped structures can be

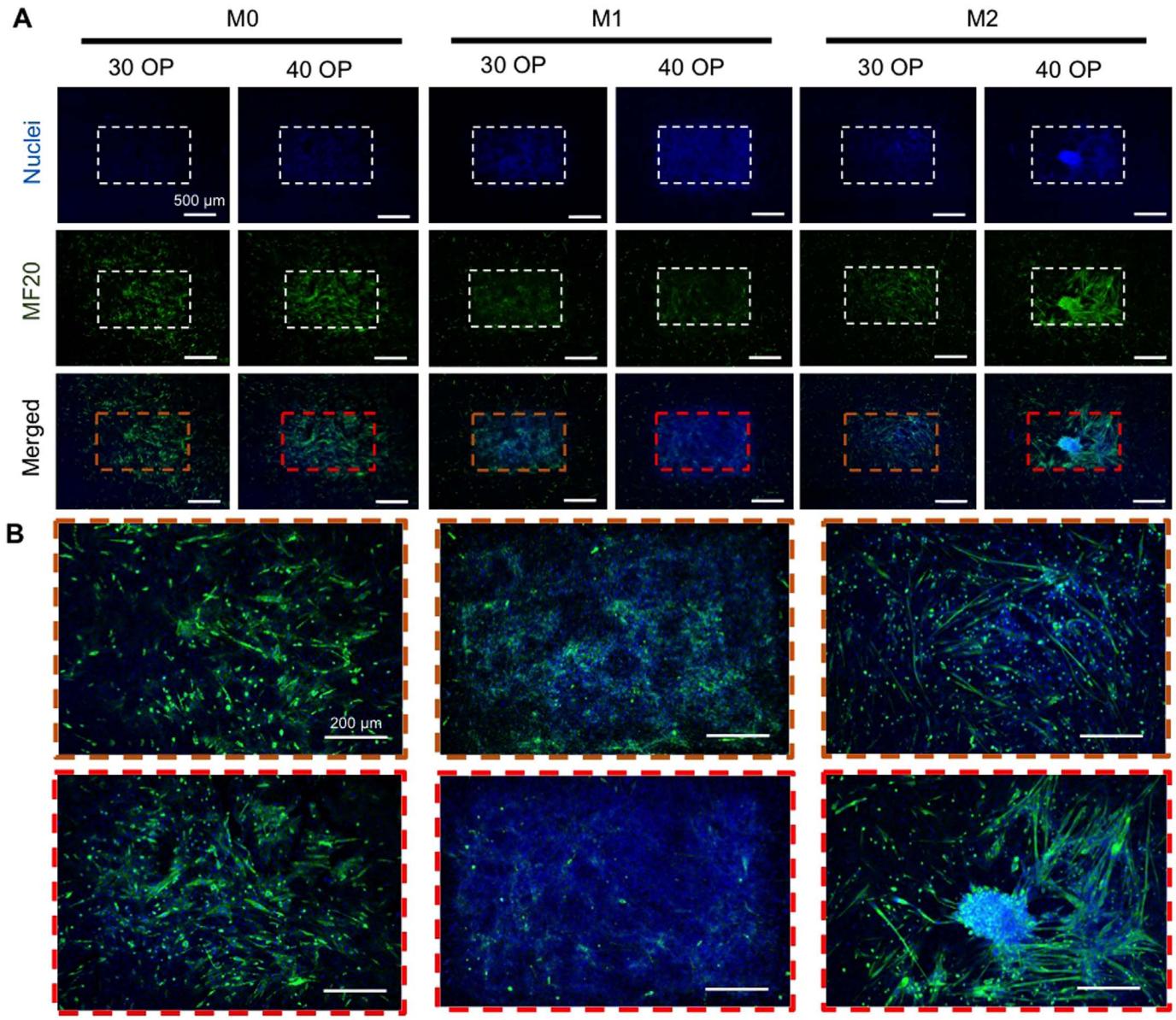

Fig. 7. Spatial control of C2C12 differentiation under enhanced magnification. (A) Representative confocal micrographs taken from data in Fig. 6 showing the effects of bioprinted exosomes on C2C12 differentiation with higher magnification. Nuclei (blue) and MF20 (green). Scale bar = 500 µm (**B**) Higher magnification micrographs of patterns in panel A. Scale bar = 200 µm.

formed using a 'layered assembly of scaffolds' process [67].

Bioprinted exosomes can signal cells *via* surface receptors and/ by delivering cargo into the cytoplasm. Here, we show that exosomes bound to collagen are readily internalized by the cells, which can be attributed to competitive binding interactions between exosomes bound to the ECM and the cell and/or cell meditated proteolysis of the substrate ECM and subsequent release of bioactive exosomes. This also allows for the fabrication of exosome microarrays, similar to cDNA array applications [68], to study cell-exosome interaction in a high-throughput manner that are not only based on surface interaction but also cellular uptake of ECM-bound extracellular vesicles.

We also demonstrated that solid-phase presentation of exosomes has similar effects as their liquid-phase counterparts, confirming their biological activity when immobilized to ECM matrix. However, this may not be the case for exosomes from different source/recipient cells, therefore more studies are required to establish whether liquid/solid phase presentation has differential effects on their biological activity. M1 derived exosomes inhibited C2C12 myogenesis, which could be attributed to a possible presence of pro-inflammatory effector cargo associated with the exosome surface and/or cargo contained within the lumen. Previous reports have shown that M1 and M2 macrophages have differential effects on myogenesis, both *in vitro* and *in vivo* [44–47,49,69]. It has been reported that M1 macrophage secretome (in conditioned media) inhibits myogenesis *in vitro via* secretion of inflammatory signaling agents, whereas conditioned media from M2 macrophages promote myotube fusion and myogenesis [45]. Moreover *in vivo* investigations suggest that pro-inflammatory M1 macrophages play a crucial role in inducing proliferation of myogenic precursor cells and angiogenesis during early phases of muscle regeneration whereas M2 macrophages induce and promote differentiation of MPCs during late stages of regeneration [47,48,70]. To our knowledge, this is the first report suggesting that such observations could be mediated, at least in part, *via* exosomes secreted by macrophages. A more in-depth molecular characterization of the cargo associated with the M1 and M2 exosome populations would be required to decipher the signaling agents associated with such observations.

5. Conclusions

Exosomes are sequestered in the microenvironment by immobilization within the ECM and/or to the cell surface resulting in spatially confined distributions of exosomes and their cell signaling cargo. Solid-phase exosomes are enabled because they exhibit inherent binding properties to ECM molecules directly or through specific binding protein intermediaries. Such observations can be translated into immobilization strategies that permit fabrication of well-defined, solid-phase exosome microenvironments needed to better understand their biology as well as to ultimately enable controlled, localized delivery of exogenous drug-loaded exosomes working synergistically with their native cargo. Toward meeting these goals, we demonstrated for the first time that engineered solid-phase exosome microenvironments, bioprinted using macrophage-derived exosomes, retained biological activity and spatially controlled stem cell differentiation. This approach will be useful for investigating the role of solid-phase exosomes in both physiologic and pathophysiologic conditions and represents a novel approach to localize exosome delivery.

Funding sources

This work was financially supported by the Dowd Fellowship at Carnegie Mellon University (SSY), Carnegie Mellon University - Biohybrid Organ Initiative and NIHR21AR072954-01 (PGC).

Appendix A. Supplementary material

Supplementary data associated with this article can be found in the online version at doi:10.1016/j.bprint.2019.e00041.

References

[1] J. Malda, J. Boere, C.H.A. Van De Lest, P.R. Van Weeren, M.H.M. Wauben, Extracellular vesicles - new tool for joint repair and regeneration, Nat. Rev. Rheumatol. 12 (4) (2016) 243–249.
[2] L.A. Mulcahy, R.C. Pink, D.R.F. Carter, Routes and mechanisms of extracellular vesicle uptake, J. Extracell. Vesicles 3 (1) (2014).
[3] M. Yáñez-Mó, et al., Biological properties of extracellular vesicles and their physiological functions, J. Extracell. Vesicles 4 (2015) (2015) 1–60.
[4] S. Mathivanan, H. Ji, R.J. Simpson, Exosomes: extracellular organelles important in intercellular communication, J. Proteom. 73 (10) (2010) 1907–1920.
[5] D. Ha, N. Yang, V. Nadithe, Exosomes as therapeutic drug carriers and delivery vehicles across biological membranes: current perspectives and future challenges, Acta Pharm. Sin. B 6 (4) (2016) 287–296.
[6] E.V. Batrakova, M.S. Kim, Using exosomes, naturally-equipped nanocarriers, for drug delivery, J. Control. Release 219 (2015) 396–405.
[7] R.C. Lai, R.W.Y. Yeo, K.H. Tan, S.K. Lim, Exosomes for drug delivery - a novel application for the mesenchymal stem cell, Biotechnol. Adv. 31 (5) (2013) 543–551.
[8] V.P. Torchilin, Recent advances with liposomes as pharmaceutical carriers, Nat. Rev. Drug Discov. 4 (2) (2005) 145–160.
[9] T.M. Allen, P.R. Cullis, Liposomal drug delivery systems: from concept to clinical applications, Adv. Drug Deliv. Rev. 65 (1) (2013) 36–48.
[10] C. Zylberberg, S. Matosevic, Pharmaceutical liposomal drug delivery: a review of new delivery systems and a look at the regulatory landscape, Drug Deliv. 23 (9) (2016) 3319–3329.
[11] K. Rilla, A.M. Mustonen, U.T. Arasu, K. Härkönen, J. Matilainen, P. Nieminen, Extracellular vesicles are integral and functional components of the extracellular matrix, Matrix Biol. (2017).
[12] S. Rieu, C. Géminard, H. Rabesandratana, J. Sainte-Marie, M. Vidal, Exosomes released during reticulocyte maturation bind to fibronectin via integrin α4β1, Eur. J. Biochem. 267 (2) (2000) 583–590.
[13] C.C. Huang, R. Narayanan, S. Alapati, S. Ravindran, Exosomes as biomimetic tools for stem cell differentiation: applications in dental pulp tissue regeneration, Biomaterials 111 (2016) 103–115.
[14] A. Németh, et al., Antibiotic-induced release of small extracellular vesicles (exosomes) with surface-associated DNA, Sci. Rep. 7 (1) (2017).
[15] W. Mu, S. Rana, M. Zöller, Host matrix modulation by tumor exosomes promotes motility and invasiveness, Neoplasia 15 (8) (2013) (p. 875–IN4).
[16] R. Garimella, et al., Extracellular membrane vesicle derived from 143b osteosarcom cells contain pro-osteoclastogenic cargo: a nove communication mechanism in osteosarcoma bone microenvironment, Transl. Oncol. 7 (3) (2014) 331–340.
[17] T. Whiteside, Tumor-derived exosomes and their role in tumor-induced immune suppression, Vaccines 4 (4) (2016) 35.
[18] T.L. Whiteside, Tumor-derived exosomes and their role in cancer progression, Adv. Clin. Chem. 74 (2016) 103–141.
[19] J. Taipale, J. Keski-Oja, Growth factors in the extracellular matrix, FASEB J. 11 (1) (1997) 51–59.
[20] E.D. Miller, G.W. Fisher, L.E. Weiss, L.M. Walker, P.G. Campbell, Dose-dependent cell growth in response to concentration modulated patterns of FGF-2 printed on fibrin, Biomaterials 27 (10) (2006) 2213–2221.
[21] J.A. Phillippi, E. Miller, L. Weiss, J. Huard, A. Waggoner, P. Campbell, Microenvironments engineered by inkjet bioprinting spatially direct adult stem cells toward muscle-and bone-like subpopulations, Stem Cells 26 (1) (2008) 127–134.
[22] E.D.F. Ker, et al., Engineering spatial control of multiple differentiation fates within a stem cell population, Biomaterials 32 (13) (2011) 3413–3422.
[23] W. Zhang, et al., Biopatterned CTLA4/Fc matrices facilitate local immunomodulation, engraftment, and glucose homeostasis after pancreatic islet transplantation, Diabetes 65 (12) (2016) 3660–3666.
[24] S. Shakir, et al., Transforming growth factor beta 1 augments calvarial defect healing and promotes suture regeneration, Tissue Eng. Part A 21 (5–6) (2015) 939–947.
[25] T. Tabata, Morphogens, their identification and regulation, Development 131 (4) (2004) 703–712.
[26] J.B. Gurdon, P.Y. Bourillot, Morphogen gradient interpretation, Nature 413 (6858) (2001) 797–803.
[27] P.C. Wilkinson, How do leucocytes perceive chemical gradients?, FEMS Microbiol. Lett. 64 (5–6) (1990) 303–311.
[28] T.A. Einhorn, Enhancement of fracture-healing, J. Bone Jt. Surg. 77 (6) (1995) (p. 940 LP-956).
[29] E.D. Miller, K. Li, T. Kanade, L.E. Weiss, L.M. Walker, P.G. Campbell, Spatially directed guidance of stem cell population migration by immobilized patterns of growth factors, Biomaterials 32 (11) (2011) 2775–2785.
[30] S. Herberg, et al., Inkjet-based biopatterning of SDF-1beta augments BMP-2-induced repair of critical size calvarial bone defects in mice, Bone 67 (2014) 95–103.
[31] C.S. Hong, et al., Circulating exosomes carrying an immunosuppressive cargo interfere with cellular immunotherapy in acute myeloid leukemia, Sci. Rep. 7 (1) (2017).
[32] M.-N. Theodoraki, S.S. Yerneni, T.K. Hoffmann, W.E. Gooding, T.L. Whiteside, Clinical significance of PD-L1 $^{+}$ exosomes in plasma of head and neck cancer patients, Clin. Cancer Res. 24 (4) (2018) 896–905.
[33] M.-N. Theodoraki, S.S. Yerneni, C. Brunner, J. Theodorakis, T.K. Hoffmann, T.L. Whiteside, Plasma-derived exosomes reverse epithelial-to-mesenchymal transition after photodynamic therapy of patients with head and neck cancer, Oncoscience 5 (3–4) (2018) 75.
[34] L. Muller, C.-S. Hong, D.B. Stolz, S.C. Watkins, T.L. Whiteside, Isolation of biologically-active exosomes from human plasma, J. Immunol. Methods 411 (2014) 55–65.
[35] N. Ludwig, S.S. Yerneni, B.M. Razzo, T.L. Whiteside, HNSCC-derived exosomes promote angiogenesis through reprogramming of 1 endothelial cells in vitro and in vivo, Mol. Cancer Res. (2018) (p. molcanres-0358).
[36] C.-S. Hong, S. Funk, L. Muller, M. Boyiadzis, T.L. Whiteside, Isolation of biologically active and morphologically intact exosomes from plasma of patients with cancer, J. Extracell. Vesicles 5 (1) (2016) 29289.
[37] W.D. Gray, A.J. Mitchell, C.D. Searles, An accurate, precise method for general labeling of extracellular vesicles, MethodsX 2 (2015) 360–367.
[38] C. Tuzmen, K. Verdelis, L. Weiss, P. Campbell, Crosstalk between substance P and calcitonin gene-related peptide during heterotopic ossification in murine Achilles tendon, J. Orthop. Res. 36 (5) (2018) 1444–1455.
[39] D.M. Smith, et al., Precise control of osteogenesis for craniofacial defect repair: the role of direct osteoprogenitor contact in BMP-2-based bioprinting, Ann. Plast. Surg. 69 (4) (2012) 485–488.
[40] J.A. Phillippi, E. Miller, L. Weiss, J. Huard, A. Waggoner, P. Campbell, Microenvironments engineered by inkjet bioprinting spatially direct adult stem cells toward muscle- and bone-like subpopulations, Stem Cells 26 (1) (2008) 127–134.
[41] P.G. Campbell, L.E. Weiss, Tissue engineering with the aid of inkjet printers, Expert Opin. Biol. Ther. 7 (8) (2007) 1123–1127.
[42] P.G. Campbell, E.D. Miller, G.W. Fisher, L.M. Walker, L.E. Weiss, Engineered spatial patterns of FGF-2 immobilized on fibrin direct cell organization, Biomaterials 26 (33) (2005) 6762–6770.
[43] E.D. Miller, G.W. Fisher, L.E. Weiss, L.M. Walker, P.G. Campbell, Dose-dependent cell growth in response to concentration modulated patterns of FGF-2 printed on fibrin, Biomaterials 27 (10) (2006) 2213–2221.
[44] M. Saclier, M. Theret, R. Mounier, B. Chazaud, Effects of macrophage conditioned-medium on murine and human muscle cells: analysis of proliferation, differentiation, and fusion, Methods Mol. Biol. 1556 (2017) 317–327.
[45] M. Saclier, et al., Differentially activated macrophages orchestrate myogenic precursor cell fate during human skeletal muscle regeneration, Stem Cells 31 (2) (2013) 384–396.
[46] M. Saclier, S. Cuvellier, M. Magnan, R. Mounier, B. Chazaud, Monocyte/macrophage interactions with myogenic precursor cells during skeletal muscle regeneration, FEBS J. 280 (17) (2013) 4118–4130.
[47] M. Bencze, et al., Proinflammatory macrophages enhance the regenerative capacity of human myoblasts by modifying their kinetics of proliferation and differentiation, Mol. Ther. 20 (11) (2012) 2168–2179.
[48] C. Latroche, et al., Coupling between myogenesis and angiogenesis during skeletal muscle regeneration is stimulated by restorative macrophages, Stem Cell Rep. 9 (6)

(2017) 2018–2033.
[49] L. Arnold, et al., Inflammatory monocytes recruited after skeletal muscle injury switch into antiinflammatory macrophages to support myogenesis, J. Exp. Med. 204 (5) (2007) 1057–1069.
[50] H.C. Anderson, "Electron microscopic studies of induced cartilage development and calcification, J. Cell Biol. 35 (1) (1967) 81–101.
[51] E. Bonucci, Fine structure of early cartilage calcification, J. Ultra. Res. 20 (1–2) (1967) 33–50.
[52] L. Huleihel, et al., Matrix-bound nanovesicles within ECM bioscaffolds, Sci. Adv. 2 (6) (2016) e1600502.
[53] L. Cui, D.A. Houston, C. Farquharson, V.E. MacRae, Characterisation of matrix vesicles in skeletal and soft tissue mineralisation, Bone 87 (2016) 147–158.
[54] H.C. Anderson, Matrix vesicles and calcification, Curr. Rheumatol. Rep. 5 (3) (2003) 222–226.
[55] L. Huleihel, et al., Matrix-bound nanovesicles recapitulate extracellular matrix effects on macrophage phenotype, Tissue Eng. Part A 23 (21–22) (2017) 1283–1294.
[56] Z. Wang, Z. Wang, W.W. Lu, W. Zhen, D. Yang, S. Peng, Novel biomaterial strategies for controlled growth factor delivery for biomedical applications, NPG Asia Mater. 9 (10) (2017).
[57] Y.S. Park, Y. Ito, "Micropattern-immobilization of heparin to regulate cell growth with fibroblast growth factor, Cytotechnology 33 (1–3) (2000) 117–122.
[58] Y. Ito, Micropattern immobilization of polysaccharide, J. Inorg. Biochem. 79 (1–4) (2000) 77–81.
[59] Y. Ito, M. Hayashi, Y. Imanishi, Gradient micropattern immobilization of heparin and its interaction with cells, J. Biomater. Sci. Polym. Ed. 12 (4) (2001) 367–378.
[60] L.E. Dickinson, S. Gerecht, Micropatterned surfaces to study hyaluronic acid interactions with cancer cells, J. Vis. Exp.: JoVE (46) (2010).
[61] S. Herberg, et al., Inkjet-based biopatterning of SDF-1β augments BMP-2-induced repair of critical size calvarial bone defects in mice, Bone 67 (2014) 95–103.
[62] P. Calvert, Inkjet printing for materials and devices, Chem. Mater. 13 (10) (2001) 3299–3305.
[63] M. Yanez-Mo, et al., Biological properties of extracellular vesicles and their physiological functions, J. Extracell. Vesicles 4 (2015) 27066.
[64] T. Lener, et al., Applying extracellular vesicles based therapeutics in clinical trials - An ISEV position paper, J. Extracell. Vesicles 4 (1) (2015).
[65] G.M. Cooper, et al., Inkjet-based biopatterning of bone morphogenetic protein-2 to spatially control calvarial bone formation, Tissue Eng. Part A 16 (5) (2010) 1749–1759.
[66] M. Geiger, R.H. Li, W. Friess, Collagen sponges for bone regeneration with rhBMP-2, Adv. Drug Deliv. Rev. 55 (12) (2003) 1613–1629.
[67] L.E. Weiss, J.W. Calvert, Assembled scaffolds for three dimensional cell culturing and tissue generation. Google Patents, 07-Nov-2000.
[68] J. Ziauddin, D.M. Sabatini, Microarrays of cells expressing defined cDNAs, Nature 411 (6833) (2001) 107–110.
[69] S.A. Villalta, H.X. Nguyen, B. Deng, T. Gotoh, J.G. Tidbal, Shifts in macrophage phenotypes and macrophage competition for arginine metabolism affect the severity of muscle pathology in muscular dystrophy, Hum. Mol. Genet. 18 (3) (2009) 482–496.
[70] M.L. Novak, E.M. Weinheimer-Haus, T.J. Koh, Macrophage activation and skeletal muscle healing following traumatic injury, J. Pathol. 232 (3) (2014) 344–355.